Real-space observations of 60-nm skyrmion dynamics in an insulating magnet under low heat flow

Xiuzhen Yu (yu_x@riken.jp)
RIKEN https://orcid.org/0000-0003-3136-7289
Fumitaka Kagawa
University of Tokyo https://orcid.org/0000-0002-1763-6799
Shinichiro Seki
University of Tokyo
Masashi Kubota
Riken,CEMS
Jan Masell
RIKEN Center for Emergent Matter Science https://orcid.org/0000-0002-9951-4452
Fehmi Yasin
RIKEN Center for Emergent Matter Science https://orcid.org/0000-0001-9382-7565
Kiyomi Nakajima
RIKEN Center for Emergent Matter Science
Masao Nakamura
RIKEN Center for Emergent Matter Science https://orcid.org/0000-0002-6812-6334
Masashi Kawasaki
Quantum-Phase Electronics Center and D
Naoto Nagaosa
The University of Tokyo/RIKEN
Yoshinori Tokura
RIKEN https://orcid.org/0000-0002-2732-4983

Article

Keywords: skyrmion dynamics, magnet, spintronics.

Posted Date: February 3rd, 2021

DOI: https://doi.org/10.21203/rs.3.rs-156692/v1

Version of Record: A version of this preprint was published at Nature Communications on August 23rd, 2021. See the published version at https://doi.org/10.1038/s41467-021-25291-2.

Real-space observations of 60-nm skyrmion dynamics in an insulating magnet under low heat flow

Xiuzhen Yu[1*], Fumitaka Kagawa[1, 2], Shinichiro Seki[2,3], Masashi Kubota[1†], Jan Masell[1], Fehmi S. Yasin[1], Kiyomi Nakajima[1], Masao Nakamura[1], Masashi Kawasaki[1, 2], Naoto Nagaosa[1, 2] and Yoshinori Tokura[1,2, 4]

[1]RIKEN Center for Emergent Matter Science (CEMS), Wako 351-0198, Japan

[2]Department of Applied Physics, University of Tokyo, Tokyo 113-8656, Japan

[3] Institute of Engineering Innovation, University of Tokyo, Tokyo 113-0032, Japan

[4]Tokyo College, University of Tokyo, Tokyo 113-8656, Japan

*Correspondence to: yu_x@riken.jp

† Present affiliation: Technology and Business Development Unit, Murata Manufacturing Co., Ltd., Kyoto 617-8555, Japan

Abstract

Thermal-current induced electron and spin dynamics in solids –dubbed "caloritronics" – have generated widespread interest in both fundamental physics and spintronics applications. Here, we examine the dynamics of nanometric topological spin textures, skyrmions, driven by a temperature gradient ∇T or heat flow. The heat-flow-drive skyrmion dynamics are evaluated through in-situ real-space observations in an insulating helimagnet Cu_2OSeO_3. We observe increases of the skyrmion velocity and the Hall angle with increasing ∇T above a critical value of ~ 13 mK/mm, which is two orders of magnitude lower than the ∇T required to drive ferromagnetic domain walls, in agreement with theoretical predictions. A comparable magnitude of ∇T is also observed to move the domain walls between a skyrmion domain and the non-topological conical-spin domain from cold to hot regions. Our results demonstrate the efficient manipulation of skyrmions by temperature gradients, a promising step towards energy-efficient "green" spintronics.

Introduction

Control and manipulation of electron spins are indispensable for the development of low energy-consumption electronic devices. Among them, electron transport phenomena induced by interaction with heat flow as known as thermal current have attracted significant attention since they promise to recycle the wasted heat facilitating green information technology. In the field of spin-caloritronics[1-2], a thermal current is associated with the spin current which induces emergent phenomena of the spin-charge coupled dynamics with related entropy[1], to name a few, spin Nernst effect[3], spin-dependent Peltier effect[4], spin Seebeck effect[5], and thermal Hall effect[6]. These thermal-current induced effects are mediated by the collective dynamics of spin textures, such as magnetic twists (domain walls) or vortex-like spin textures, coupled with a spin current J_S converted from the thermal current[7]. Due to the conservation of total angular momentum in the system, the thermal current can in turn exert a torque on the spin texture that leads to temperature-gradient induced spin texture dynamics[8-9]. In analogy to current-driven spin texture motions[10-11], temperature-gradient induced magnetization dynamics have been reported in metallic systems via spin transfer torque on magnetic domain walls[12].

In magnetically ordered insulators, however, charge currents are absent. Still, a temperature gradient can drive magnetic textures in insulating ferromagnets (FM) [13-14] via the transfer of spin angular momentum of the thermally induced magnon current, similar to the conduction electron spin transfer torque mechanism in metallic FM. The possibility of inducing magnon currents and relatively smaller Gilbert damping constant in insulating FM is attracting considerable attention for energy efficient manipulations of spin textures.

Compared with topologically-trivial spin textures like FM domain wall, vortex-like topological spin textures, e.g. magnetic skyrmions, are expected to move with lower temperature gradients ∇T due to their topological nature, which is advantageous for low energy-consumption in

electronic devices[15-20]. In particular, skyrmions emerging in insulating materials are attractive for applications that require low energy dissipation. The magnon current j_x in the lateral direction produces a skyrmion velocity as described by[21]

$$v_x = v_x^M - v_x^B \quad (1)$$

$$v_y = 2\alpha\eta Q v_x^M \quad (2)$$

where $v_x^M = \gamma J a^2 j_x$ is the velocity due to the magnon current, and

$$v_x^B = (\frac{\gamma}{\pi Q^2})\alpha\eta a^2 k_B \nabla T \quad (3)$$

is that due to Brownian motion. Here a, J, α and γ are the lattice constant, the exchange coupling constant, the Gilbert damping constant and the gyromagnetic ratio, and $k_B, \nabla T$ and η are the Boltzmann constant, the temperature gradient, and a constant of order unity, respectively. The Q is the skyrmion number (integer topological charge), as defined by

$$Q = \frac{1}{4\pi}\int M \cdot \left(\frac{\partial M}{\partial x} \times \frac{\partial M}{\partial y}\right) dxdy\,. \quad (4)$$

Here M is the unit vector of local magnetization in the related materials. When the Gilbert damping constant α is small, the Brownian motion can be neglected compared to the magnon-driven skyrmion motion[22].

Among insulating magnets, the helimagnet Cu_2OSeO_3 hosting 60-nm skyrmions is a good target material[23] to manipulate topological spin textures with an electric field[24-26] owing to its intrinsic magnetoelectric coupling. In addition, thermally driven unidirectional rotation of a skyrmion lattice (SkL) has been demonstrated in a thin plate of Cu_2OSeO_3 under the presence of radial thermal current.[27] The next step in exploring such thermally driven skyrmion dynamics is to understand the drift motion of isolated skyrmions or skyrmion clusters in a spin-polarized background under a linear ∇T, and to quantitatively evaluate the threshold ∇T for driving skyrmions. Similar to the thermal control of FM domain walls in an insulator, skyrmion dynamics with a magnon current have been numerically predicted in several studies[21, 28-31]. The results

indicate that skyrmions move from cold to hot regions via a magnonic spin transfer torque, in the opposite direction of the magnon flow. However, these predictions have yet to be observed.

Here, we apply ∇T to a thin plate of Cu_2OSeO_3 crystal equipped with a heater and thermometers and use Lorentz transmission electron microscopy (TEM) to perform in-situ real-space observations of the proliferation and drift motion of 60-nm skyrmions and evaluate their dynamics under the low ∇T.

Results

Thermally-driven skyrmion motions in a designed microdevice composed of an insulating magnet

Cu_2OSeO_3 has a chiral-lattice structure as shown in Fig. 1**a**. The hexagonal SkL can be generated under the specific field and temperature conditions, as exemplified by an over-focus Lorentz TEM image taken at 20 K under a normal magnetic field of 60 mT (Fig. 1**b**). To investigate the skyrmion dynamics under temperature gradients, we have prepared a Cu_2OSeO_3 thin plate with a heater (H) and thermometers (R1 and R2) composed of the meander Pt pattern (the size: l (length in total) = 2.34 mm, w (width) = 2.1μm and t (thickness) = 25 nm) on the top surface of the plate having a partially thinner region for electron beam transmission, as shown in Figs. 1**c**-1**d**; the top (**c**) and cross-section (**d**) views, respectively. Figure 1**e** is a schematic drawing of skyrmion flows under ∇T in lateral direction, illustrating that a skyrmion moves from cold region to hot region against the heat flow and exhibits simultaneously Hall motion.

Realizations of various magnetic configurations including skyrmions in the microdevice

Figure 2 represents the externally applied magnetic-field (B)−temperature (T) phase diagram (Fig. 2 **a**) and corresponding magnetic configurations of the 100 nm thick Cu_2OSeO_3 plate (Figs. 2**b**-2**g**) measured by systematic Lorentz TEM observations at various T and B applied normally to the thin plate. Multiple domains of the in-plane helices (stripes in Fig. 2**b**) appear in the initial

state, as we increase the field *B*, mixed spin textures emerge, such as coexisting helices (H) and SkL (Figs. 2**c-2d**), and SkL coexistent with a conical (C) domain (Fig. 2**f**). The nearly perfect SkL can only be generated under proper *T* and *B* conditions (Fig. 2**e**), and a FM state (spin polarized state) dominates under a higher external field (Fig. 2**g**). (Note here that Lorentz TEM gives monotonic contrast for the vertical C structure and FM state.) In the following, we have chosen mixed states consisting of skyrmions and C or FM domains to probe the temperature-gradient effect on skyrmions.

Skyrmion dynamics in the microdevice under low heat flows

Figures 3**a**-3**b** show two isolated islands of skyrmions observed before (**a**) and during (**b**) a 10-μA-current excitation on the heater at an indicated elapsed time (100 ms), respectively. The center position of the skyrmion island does not change significantly in spite of the change of orientations (indicated by yellow and orange dashed lines in Figs. 3a-3b, respectively) of its hexagonal lattice during the current excitation. Figures 3**c**-3**d** show two snapshots of over-focus Lorentz TEM images for a mixed state with a skyrmion domain and possible vertical-C domain (monotonic contrast in the images), observed before (**c**) and during (**d**) a 50-μA-current excitation at an elapsed time of 20 ms, respectively. The facets of the hexagonal lattice of skyrmions as the domain walls between skyrmion domain and C domain, indicated by yellow dashed lines in Fig. 3**c**, drift from the cold region to the hot region (right side), accompanying a constriction of the C domain and a possible proliferation of metastable skyrmions or flows of skyrmions from the thicker region on the left-outside to the right-inside of the Lorentz TEM view. The latter is difficult to confirm due to electron wave amplitude loss in the thicker sample region (no TEM contrast). When the heater current is tuned off, the domain walls almost come back to the initial state (Fig. 3**c**), accompanying the replacements of metastable skyrmions by C domain or the movements of skyrmions from the view area to the left-outside of the view, indicating reversible skyrmion dynamics with heat flow shown here. The abovementioned observations have

demonstrated that skyrmion drift motion is non-zero as a function of heat flow (see also supplementary Figure 1 and an *in-situ* Lorentz TEM movie, supplementary Movie 1 in supplementary information (SI)) only for the heater currents $I_H \geq 50$ μA. Upon further increase of the heater current up to 100 μA, we clearly discern the skyrmion translational motion, as shown in Figs. 3**e**-3**g**. At the initial state, two isolated skyrmion islands encircled by yellow and blue dashed lines, respectively, were stabilized in different regions of the device (Fig. 3**e**). When we excite the heater with a 100-μA current, the left island starts to move towards the right one (Fig. 3**f**), and finally unites with the right island to flow towards the hot region (right side) of the device (Fig. 3**g** and supplementary Movie 2).

According to the abovementioned real-space observations, skyrmions in Cu_2OSeO_3 can be driven by a low heat power, P ($I_H^2 \times R$) ~10 μW (I_H = 50 μA, R = 3800 Ω). Such small heat generation does not induce appreciable changes of resistances of two thermometers R_1 and R_2 (see supplementary Figure 2) and hence can hardly characterize the ∇T in Lorentz TEM view area by resistance measurements. Therefore, to evaluate ∇T in the Lorentz TEM view area with varying I_H in the experimental setup here, we have simulated the ∇T in the view area as well as the thicker bulky part of the Cu_2OSeO_3 in terms of the finite element method (see Methods). Figure 3**h** shows the simulated temperature map of the device under 50-μA excitation on the heater; Figure 3**i** shows related temperature gradients in the Lorentz TEM view area (red line) and the thicker bulky part (black line) of the Cu_2OSeO_3 plate, respectively. It indicates that, in the present parameter set (see details in methods), the ∇T is approximately 13 mK/mm in the thinner Lorentz TEM view area, several times larger than that (~2 mK/mm) in the thicker region of the Cu_2OSeO_3 plate under 50-μA excitation on the heater. Figure 3**j** represents the ∇T–profile as a function of heater current I_H. To deduce skyrmion dynamics with varying ∇T, the *in-situ* Lorentz TEM data were obtained with a 5-ms exposure time (recording speed of 200-fps (frames

per second)), and 160-mT magnetic field applied normally to the Cu_2OSeO_3 plate. Using the calculated values of ∇T and the systematic *in-situ* Lorentz TEM observations with varying $I_{H,}$ we plotted the velocity (v) (red square symbols) and Hall angle (blue triangular symbols, defined as an angle between the heat flow and skyrmion flow directions (see Fig. 3**d**)) of the skyrmions with respect to ∇T, as shown in Fig. 3**k**; the results were obtained by tracking the cusp point of the skyrmion domain (see Figs. 3**c**-3**d** and supplementary Figure 1). The Hall motion in the upward direction and the sliding motion in the opposite direction of heat flow can be clearly discerned. Both the Hall angle and v increase nonlinearly with increasing ∇T and the v is ~ 0.1 mm/s at the critical ∇T ~ 13 mK/mm.

Discussion

The abovementioned experimental results agree well with our theoretical estimations. Nominally, the magnon current is given by[21, 30]

$$j_x = \int v_x(k)\delta f(k)\frac{d^d k}{(2\pi)^d}, \tag{5}$$

where $v_x(k) = \frac{\partial \epsilon(k)}{\hbar \partial k_x}$ is the velocity of a magnon with momentum k, and $\delta f(k) = \tau v_x \frac{\partial f_0}{\partial \epsilon}\frac{\nabla T}{T}$ is the non-equilibrium distribution correction. Here, τ is the magnon lifetime, ϵ its energy, $f_0 = (\exp\left(\frac{\epsilon}{k_B T}\right) - 1)^{-1}$ the Bose-Einstein distribution, d the dimensionality of the material system, and T the temperature. For a temperature $T = 20$ K and the Gilbert damping of the order $\alpha \sim 10^{-3}$ (Ref. 32), we roughly estimate the magnon-induced velocity of skyrmions

$$v \approx 2 \cdot 10^{-3} \nabla T \, (\frac{mm}{s}). \tag{6}$$

The critical temperature gradient is therefore evaluated as $\nabla T \approx 50$ mK/mm if the velocity of skyrmion is $v = 0.1$ mm/s, which is of the same order as the value in the present experimental setup.

In summary, we have demonstrated the dynamics of small-size (60-nm) skyrmions driven by a temperature gradient (∇T) across thin plates composed of insulating Cu_2OSeO_3 using real-space Lorentz TEM imaging. We observed the drift of the domain wall between the non-topological magnetic structure and a skyrmion domain, as well as the propagation of skyrmions under the low ∇T. We found that the velocity and Hall angle of skyrmions increase with increasing ∇T in the low thermal-current regime and report a threshold value of $\nabla T \sim$ 13 mK/mm which is two orders of magnitude smaller than that needed to drive conventional FM domain walls.

References

1. Bauer, G. E. W., MacDonald, A. H. & Maekawa, S. Spin caloritronics. *Solid State Commun*. **150**, 459-460 (2010).
2. Bauer, G. E. W., Saitoh, E. & Wees, B. J. Spin caloritronics. *Nat. Mater.* **11**, 391-399 (2012).
3. Sheng, P., et al. The spin Nernst effect in tungsten. *Sci. Adv.* **3**, e1701503 (2017).
4. Flipse, J., Bakker, F. L., Slachter, A., Dejene, F. K. & Wees, B. J. Direct observation of the spin-dependent Peltier effect. *Nat. Nanotechnol.* **7**, 166-168 (2012).
5. Uchida, K., et al. Observation of the spin Seebeck effect. *Nature* **455**, 778-781 (2008).
6. Park, S. J., Nagaosa, N. & Yang, B-J. Thermal Hall effect, spin Nernst effect, and spin density induced by a thermal gradient in collinear ferrimagnets from magnon-phonon interaction. *Nano Lett.* **20**, 2741-2746 (2020).
7. Takezoe, Y., Hosono, K., Takeuchi, A. & Tatara, G. Theory of spin transport induced by a temperature gradient. *Phys. Rev. B* **82**, 094451 (2010).
8. Hertel, R., Wulfhekel. W. & Kirschner, J. Domain-wall induced shifts in spin waves. *Phys. Rev. Lett.* **93**, 257202 (2004).
9. Han, D-S., et al. Magnetic domain-wall motion by propagating spin waves. *Appl. Phys. Lett.* **94**, 112502 (2009).
10. Yamaguchi, A., et al. Real-space observation of current-driven domain wall motion in submicron magnetic wires. *Phys. Rev. Lett.* **92**, 077205 (2004).
11. Marrows, C. H. Spin-polarized currents and magnetic domain walls. *Adv. Phys.* **54**, 585-713 (2005).
12. Chico, J., et al. Thermally driven domain-wall motion in Fe on W (110). *Phys. Rev. B* **90**, 014434 (2014).
13. Kajiwara, Y., et al. Transmission of electrical signals by spin-wave interconversion in a magnetic insulator. *Nature* **462**, 262-266 (2010).

14. Jiang, W., et al. Direct imaging of thermally driven domain wall motion in magnetic insulators. *Phys. Rev. Lett*. **110**, 177202 (2013).

15. Nagaosa, N. & Tokura, Y. Topological properties and dynamics of magnetic skyrmions. *Nat. Nanotechnol*. **8**, 899–911 (2013).

16. Jonietz, F., et al. Spin transfer torques in MnSi at ultralow current densities. *Science* **330**, 1648–1651 (2010).

17. Sampaio, J., Cros, V., Rohart, S., Thiaville, A. & Fert, A. Nucleation, stability and current induced motion of isolated magnetic skyrmions in nanostructures. *Nat. Nanotechnol*. **8**, 839–844 (2013).

18. Woo, S., et al. Observation of room-temperature magnetic skyrmions and their current-driven dynamics in ultrathin metallic ferromagnets. *Nat. Mater.* **15**, 501–506 (2016).

19. Yu, X. Z., et al. Motion tracking of 80-nm-size skyrmions upon directional current injections. *Sci. Adv.* **6**. eaaz9744 (2020).

20. Zazvorka, J., et al. Thaermal skyrmion diffusion used in a reshuffle device. *Nat. Nanotechnol*. **14**, 658–661 (2019).

21. Kong, L. & Zang, J. Dynamics of an insulating skyrmion under a temperature gradient. *Phys. Rev. Lett.* **111**, 067203 (2013).

22. Schütte, C., Iwasaki, J., Rosch, A. & Nagaosa, N. Inertia, diffusion, and dynamics of a driven skyrmion. *Phys. Rev. B* **90**, 174434 (2014).

23. Seki, S., Yu, X. Z., Ishiwata, S. & Tokura, Y. Observation of skyrmions in a multiferroic material. *Science* **336**, 198-201 (2012).

24. White, J. S., et al. Electric field control of the skyrmion lattice in Cu_2OSeO_3. *J. Phys.: Condensed Matter* **24**, 432201 (2012).

25. Huang, P., et al. In situ electric field skyrmion creation in magnetoelectric Cu_2OSeO_3. *Nano Lett.* **18**, 5167–5171 (2018).

26. Okamura, Y., Kagawa, F., Seki, S. & Tokura, Y. Transition to and from the skyrmion lattice phase by electric fields in a magnetoelectric compound. *Nat. Commun.* **7**, 12669 (2016).
27. Mochizuki, M., et al. Thermally driven ratchet motion of a skyrmion microcrystal and topological magnon Hall effect. *Nat. Mater.* **13**, 241-246 (2014).
28. Iwasaki, J., Beakman, A. J. & Nagaosa, N. Theory of magnon-skyrmion scattering in chiral magnets. *Phys. Rev. B* **89**, 064412 (2014).
29. Lin, S-Z., Batista, C. D., Reichhardt, C. & Saxena, A. ac Current generation in chiral magnetic insulators and skyrmion motion induced by the spin Seebeck effect. *Phys. Rev. Lett.* **112**, 187203 (2014).
30. Kovalev, A. A. Skyrmionic spin Seebeck effect via dissipative thermomagnonic torques. *Phys. Rev. B* **89**, 241101 (R) (2014) and *Phys. Rev. B* **91**, 239903 (2015).
31. Zhang, X., et al. Motion of skyrmions in nanowires driven by magnonic momentum-transfer forces. *New J. Phys*. **19**, 065001 (2017).
32. Seki, S. et al. *Phys. Rev. B* **93**, 235131 (2016).
33. Prasai, N. et al. *Phys. Rev. B* **99**, 020403 (2019).

Supplementary Information is available with the online version of the paper.

Acknowledgments

The authors thank Sadamichi Maekawa, Max Hirschberger, and Naoki Ogawa for fruitful discussions. This work was supported in part by Grants-In-Aid for Scientific Research (A) (Grant No. 19H00660) from Japan Society for the Promotion of Science (JSPS), JSPS program (project No. 19F19815) and the Alexander von Humboldt foundation, and Japan Science and Technology Agency (JST) CREST program (Grant Number JPMJCR1874, Grant Number JPMJCR20T1), Japan.

Author Contributions

X. Y., M. Kawasaki, N. N. and Y.T. conceived the project. X. Y. performed Lorentz TEM observations, analysed the experimental data and wrote the manuscript with Y.T.. J.M. and N.N. contributed to the theoretical analyzations. S. S. synthesized the bulky Cu_2OSeO_3. X. Y., F. K., M. Kubota, M.N., F.S.Y., and K.N. prepared devices and characterized temperature gradients in devices. All authors discussed the data and commented on the manuscript.

Competing interests

The authors declare no competing financial interest.

Author Information

Correspondence and requests for materials should be addressed to X. Z. Yu (yu_x@riken.jp).

Data availability

The data that support the plots in this paper and other findings of this study are available from the corresponding author upon reasonable request.

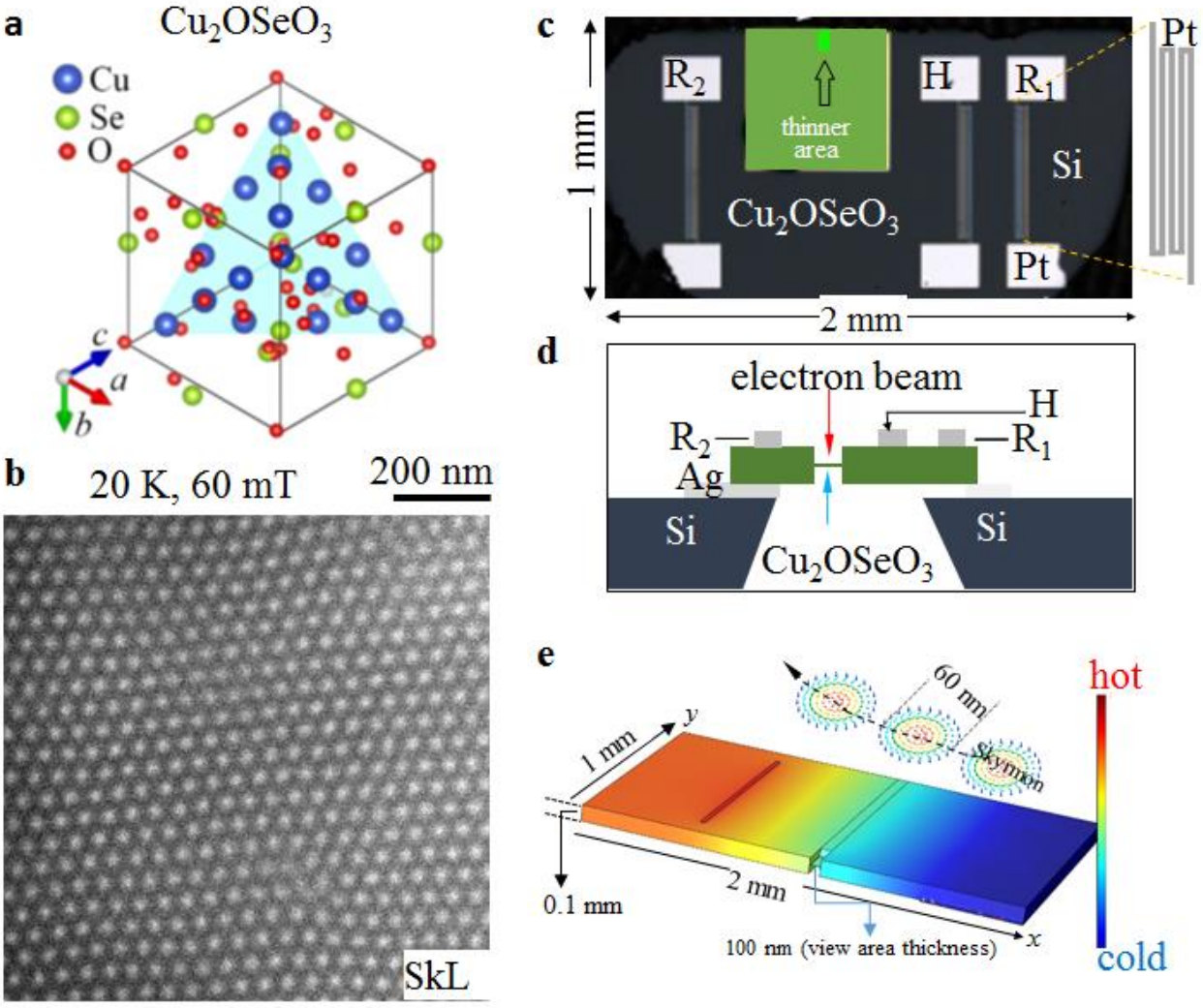

Figure 1 Thermally-driven magnetic skyrmion motion in an insulating magnet Cu_2OSeO_3 with chiral-lattice structure. a. Schematic crystal structure of the Cu_2OSeO_3. **b**. A skyrmion (white dot-like contrasts) lattice (SkL) observed by Lorentz transmission electron microscopy (TEM) in a (111) Cu_2OSeO_3 thin plate under a normal 60-mT field at 20 K. **c**, **d**. Device configurations (**c**, topography of the device; **d**, schematic of the device cross-section) for imaging skyrmion dynamics with heat flows. **e**. Schematics of skyrmion flows in the thin plates with temperature gradients (∇T). Dashed arrows indicate the anticipated trace of a skyrmion.

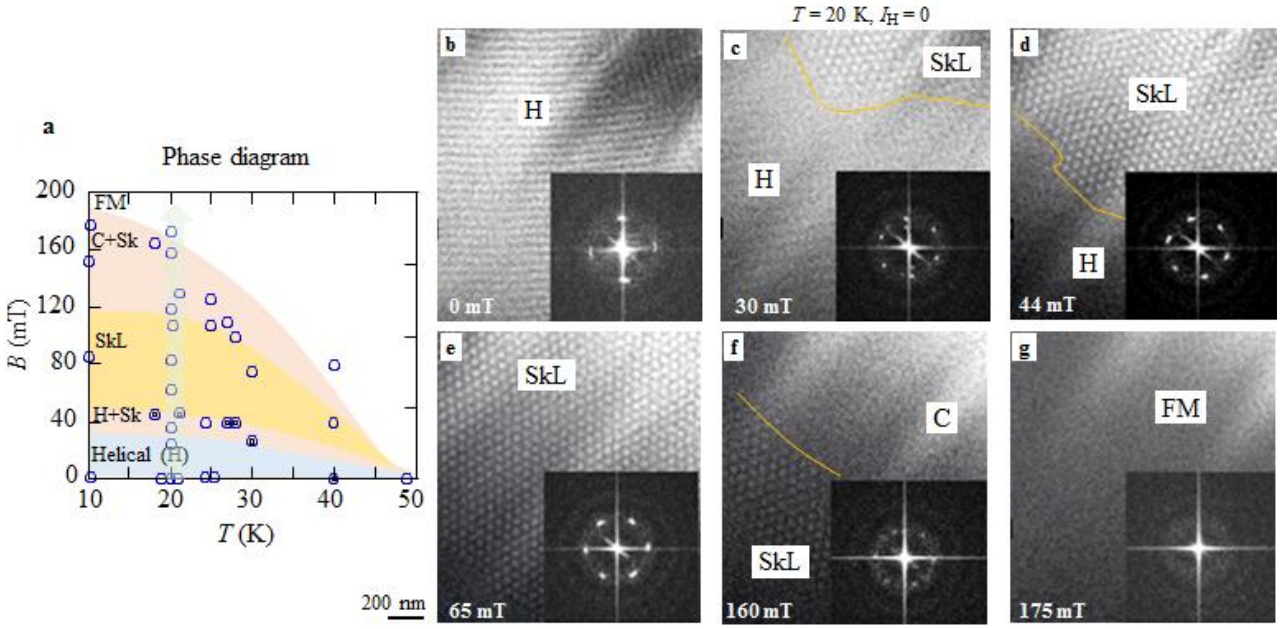

Figure 2 The temperature (*T*)-magnetic field (*B*) phase diagram observed in Cu_2OSeO_3 by Lorentz TEM. **a**. The *T*-*B* phase diagram of magnetic structure in the (111) 100 nm thick Cu_2OSeO_3 thin plate. Circles specify the *T* and *B* conditions. H, C, and FM stand for the helical, conical, and field-aligned ferromagnetic structures, respectively. **b- g**. Lorentz TEM images and their fast Fourier transforms (FFTs) observed at 20 K with increasing magnetic field.

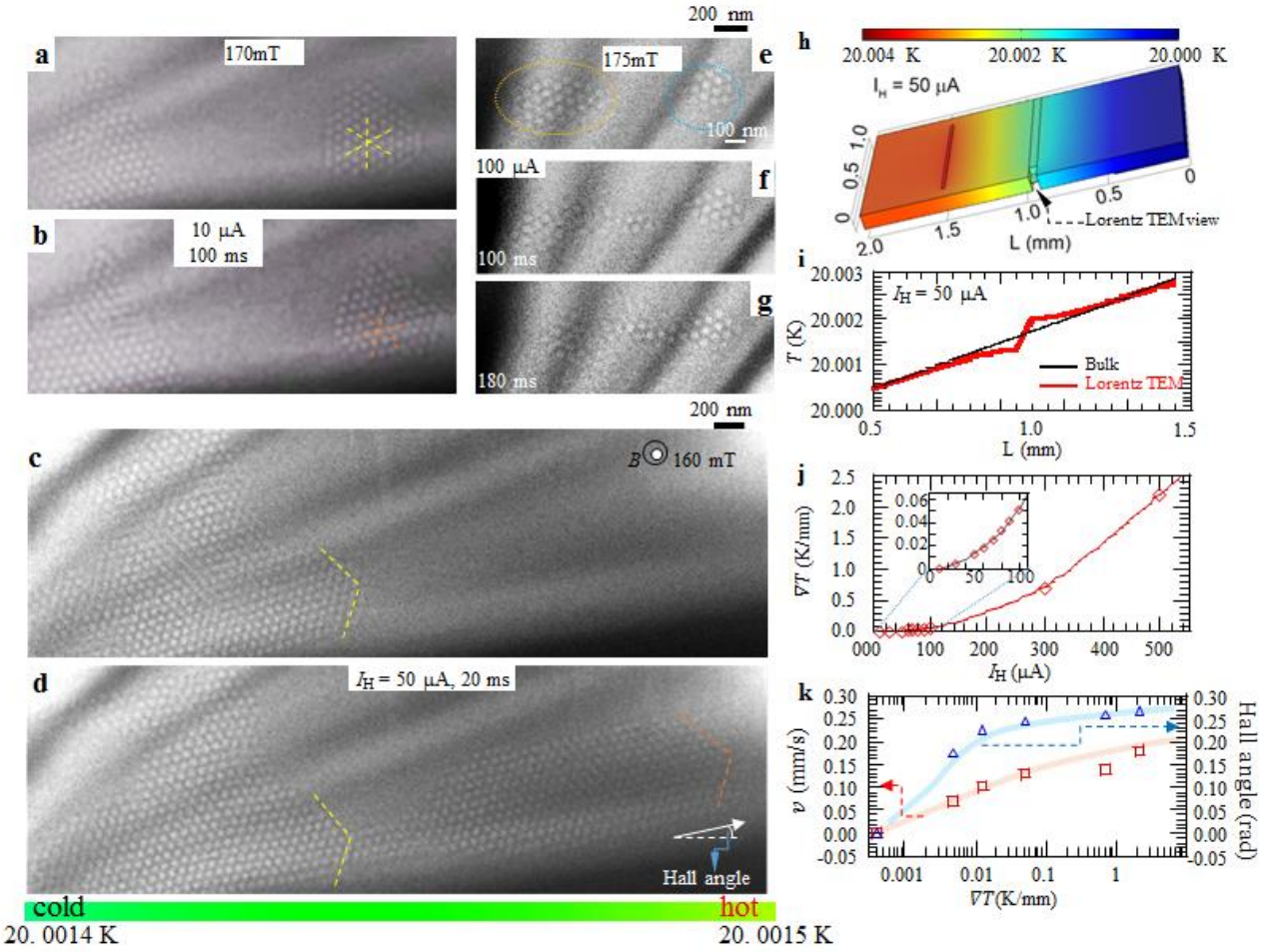

Figure 3 Heat flow-driven skyrmion motion in a Cu_2OSeO_3 thin plate. a-b. Lorentz TEM images observed before (**a**) and during (**b**) a 10-μA current flowing through the heater. **c.** Skyrmion (white dot) domain coexistent with a vertical C domain (monotonic contrast) observed under a normal field of 160 mT at 20 K in the (111) thin Cu_2OSeO_3. The boundaries between the skyrmion domain and C domain are signed by yellow dashed lines. **d**. The domain boundaries (indicated by yellow dashed lines) between skyrmions and C domain drift from the lower left to the upper right (indicated by orange dashed lines) when a 50-μA current flows through the heater (H) set on the right side of the device (see Figs. 1**c**-1**d**). **e-g**. The left skyrmion island (encircled by a dotted yellow line) flows towards the right one (dotted blue line) with 100-μA current flow. **h**. *T*-map of the thin Cu_2OSeO_3 during a 50-μA current flow. Color bar indicates the *T*-scale. **i**. Line profiles of ∇T in the Lorentz TEM view area (the rad line) and in the bulky Cu_2OSeO_3 (thicker regions, the black line) at I_H = 50 μA. **j**. Calculated ∇T versus I_H in the Lorentz TEM

view area. The inset is an enlargement of the ∇T-profile at a range of I_H from 0 to100 μA. **k**. Variation of the velocity (red squares) of the domain wall (boundary between skyrmion domain and C domain) and Hall angle (blue triangular) of the front skyrmion at the boundary with an increase of ∇T, observed while holding a constant field of 160 mT. The pink and blue lines are eye guides for the changes of the velocity and Hall angle, respectively.

Methods

Sample preparation and Lorentz TEM observations

The heater and thermometers made of meander Pt pads (see Figs.1**c**) were put on the top of a Cu_2OSeO_3 plate by depositing Pt film on the surface of Cu_2OSeO_3 and then by patterning and etching Pt film using electron lithography. To perform *in-situ* Lorentz TEM observations for the $Cu_2OSeO_3$with heat flows, the plate was partially thinned down to 100 nm thick by a focused ion beam system (NB5000, Hitachi), and then was fixed on the Si-substrate which was settled on the TEM sample holder with electrodes.

All the real space observations of skyrmions in the plate were carried out at the Lorentz TEM mode after zero-field cooling by using a multifunctional TEM (JEM-2800), which is equipped with a fast-imaging system (Gatan, OneView) and a single-tilt liquid He sample holder (Gatan, HLTST) with 10 electric terminals connected to three power sources (Keithley, 2612B). In the defocused Lorentz TEM images, skyrmions appear as bright/dark dots in the overfocused/underfocused Lorentz TEM images, reflecting their nature of clockwise spin helicity in the Cu_2OSeO_3 (see ref. 23).

Simulations of temperature maps in devices under heat flows

In the finite element simulations of temperature gradient of the present Cu_2OSeO_3, we used a commercially available software, COMSOL Multiphysics (COMSOL Inc.). To mimic the real device structure (Figs. 1**c-d**), we constructed a model: the bottom of one side of the thin plate is contacted with a "cold bath" (T = 20 K) and that of the opposite side is floated from the bath. The thermal conductivity and specific heat of Cu_2OSeO_3 are set to be typical 20-K values according to the literature[33] ; they are 40 W/m· K and 4 J/mol· K, respectively. The resistance heater is put on the surface of the floating side, and its resistance value is set to be 3800 Ω (the measured

value). The spatial profile of the temperature is thus calculated for the case that d.c. current of 10 μA –500 μA is applied to the resistance heater.

Figures

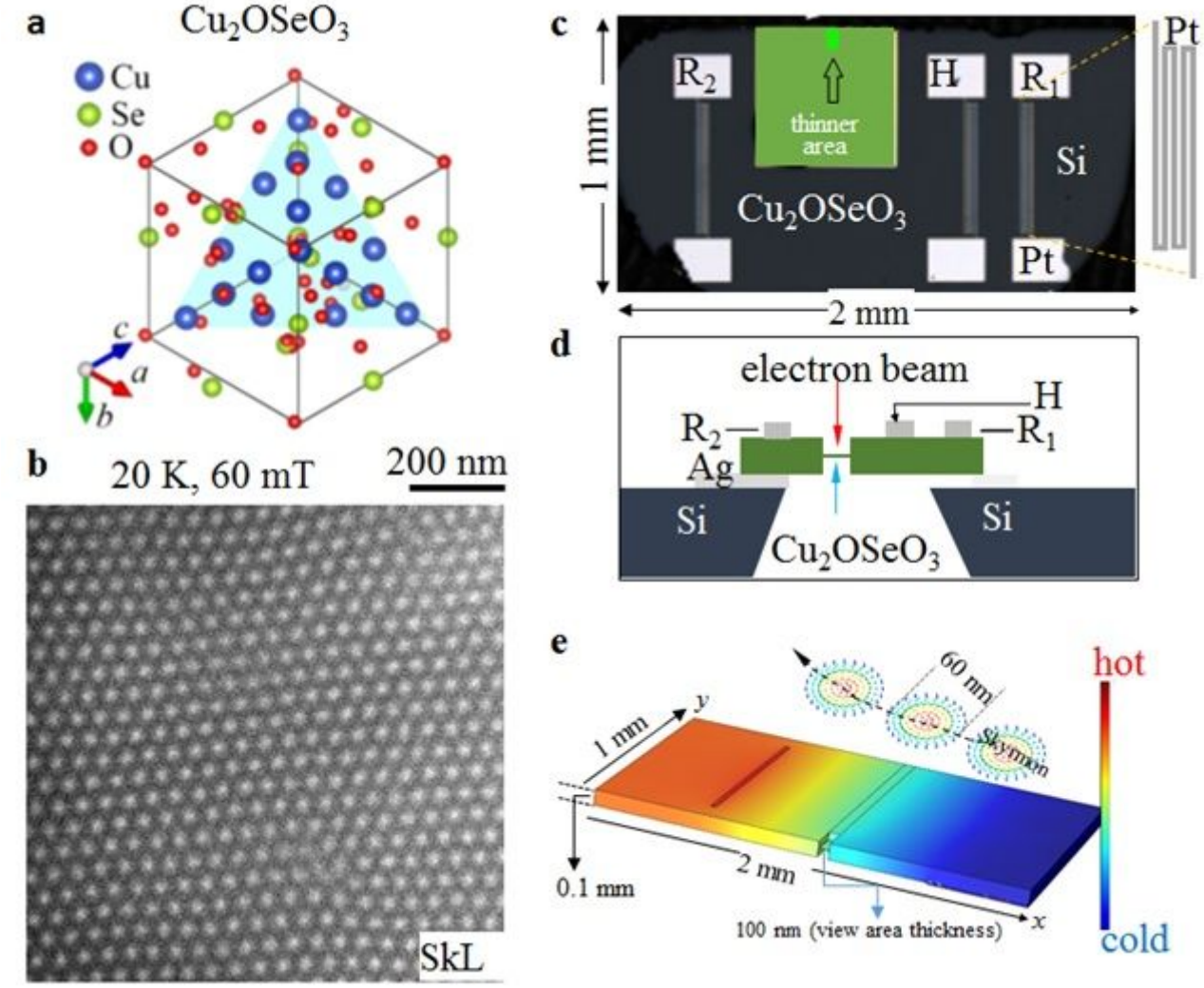

Figure 1

Thermally-driven magnetic skyrmion motion in an insulating magnet Cu2OSeO3 with chiral-lattice structure. a. Schematic crystal structure of the Cu2OSeO3. b. A skyrmion (white dot-like contrasts) lattice (SkL) observed by Lorentz transmission electron microscopy (TEM) in a (111) Cu2OSeO3 thin plate under a normal 60-mT field at 20 K. c, d. Device configurations (c, topography of the device; d, schematic of the device cross-section) for imaging skyrmion dynamics with heat flows. e. Schematics of skyrmion flows in the thin plates with temperature gradients (∇T). Dashed arrows indicate the anticipated trace of a skyrmion.

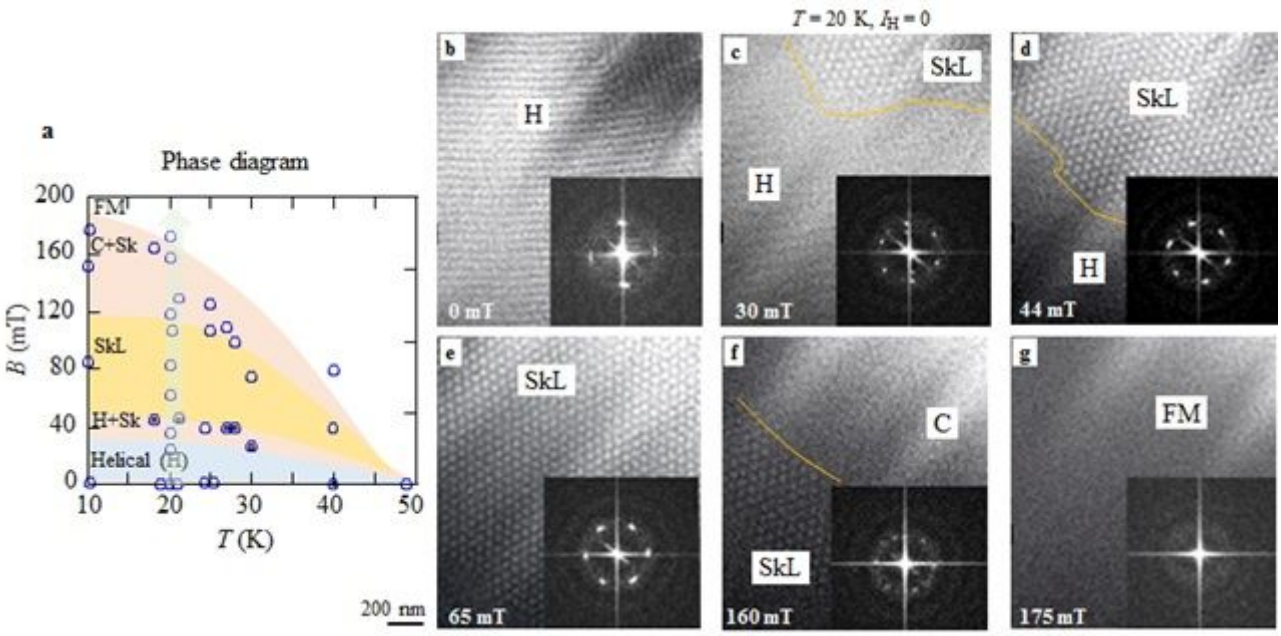

Figure 2

The temperature (T)-magnetic field (B) phase diagram observed in Cu2OSeO3 by Lorentz TEM. a. The T-B phase diagram of magnetic structure in the (111) 100 nm thick Cu2OSeO3 thin plate. Circles specify the T and B conditions. H, C, and FM stand for the helical, conical, and field-aligned ferromagnetic structures, respectively. b- g. Lorentz TEM images and their fast Fourier transforms (FFTs) observed at 20 K with increasing magnetic field.

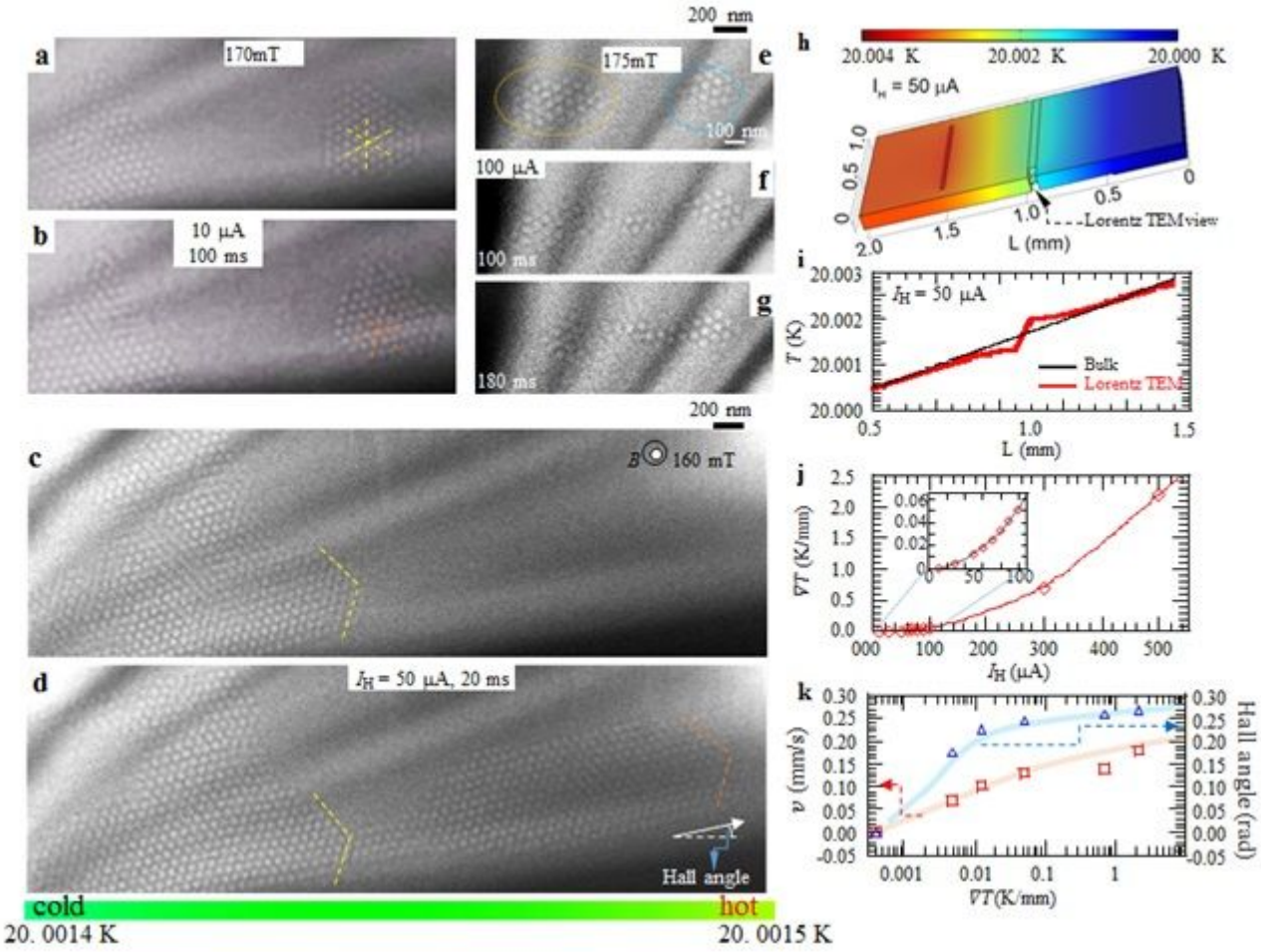

Figure 3

Heat flow-driven skyrmion motion in a Cu2OSeO3 thin plate. a-b. Lorentz TEM images observed before (a) and during (b) a 10-μA current flowing through the heater. c. Skyrmion (white dot) domain coexistent with a vertical C domain (monotonic contrast) observed under a normal field of 160 mT at 20 K in the (111) thin Cu2OSeO3. The boundaries between the skyrmion domain and C domain are signed by yellow dashed lines. d. The domain boundaries (indicated by yellow dashed lines) between skyrmions and C domain drift from the lower left to the upper right (indicated by orange dashed lines) when a 50-μA current flows through the heater (H) set on the right side of the device (see Figs. 1c-1d). e-g. The left skyrmion island (encircled by a dotted yellow line) flows towards the right one (dotted blue line) with 100-μA current flow. h. T-map of the thin Cu2OSeO3 during a 50-μA current flow. Color bar indicates the T-scale. i. Line profiles of ΔT in the Lorentz TEM view area (the rad line) and in the bulky Cu2OSeO3 (thicker regions, the black line) at IH = 50 μA. j. Calculated ΔT versus IH in the Lorentz TEM view area. The inset is an enlargement of the ΔT-profile at a range of IH from 0 to100 μA. k. Variation of the velocity (red squares) of the domain wall (boundary between skyrmion domain and C domain) and Hall angle (blue triangular) of the front skyrmion at the boundary with an increase of ΔT, observed while holding a constant field of 160 mT. The pink and blue lines are eye guides for the changes of the velocity and Hall angle, respectively.

Supplementary Files

This is a list of supplementary files associated with this preprint. Click to download.

- skyrmionmotionunderheatflowsSIyu210127.docx
- 0.05mA160mT.mp4
- 175mT0.1mA.mp4